

Simultaneous grain boundary migration and grain rotation

M. Upmanyu^{a,*}, D.J. Srolovitz^b, A.E. Lobkovsky^{c,d}, J.A. Warren^d, W.C. Carter^e

^a *Simulation and Theory of Atomic-Scale Material Phenomena (stAMP), Division of Engineering, Materials Science Program, Colorado School of Mines, 325 Brown Building, 1610 Illinois Street, Golden, CO 80401, USA*

^b *Department of Mechanical and Aerospace Engineering, Princeton University, Princeton, NJ 08540, USA*

^c *Department of Earth, Atmospheric and Planetary Sciences, Massachusetts Institute of Technology, Cambridge, MA 02139, USA*

^d *Metallurgy Division and Materials Science and Engineering Laboratory, NIST, Gaithersburg, MD 20899, USA*

^e *Department of Materials Science and Engineering, Massachusetts Institute of Technology, Cambridge, MA 02139, USA*

Received 10 June 2005; received in revised form 9 November 2005; accepted 10 November 2005

Available online 28 February 2006

Abstract

The energy of a polycrystalline network can be reduced by both grain boundary migration and grain rotation. We perform a series of molecular dynamics (MD) simulations of a circular grain embedded in an otherwise single-crystal matrix and monitor both the grain size and the misorientation of the two grains as a function of time. The MD simulations show that grain boundary migration and grain rotation occur simultaneously. The grains rotate toward local minima or cusps in the grain boundary energy versus misorientation plots. The rate of rotation decreases with increasing grain size. The boundary migration rate is a maximum at the orientations corresponding to cusps in the boundary energy. We use the MD results to fit parameters in a sharp interface limit of a phase field model of simultaneous grain boundary migration and grain rotation. With this parameterization, the phase field model is able to reproduce simultaneously the time dependence of the grain size and misorientation of the initially circular grain. The MD simulations are consistent with the phase field prediction of the grain size dependence of the rotation rate. The implications of the results for grain growth are discussed.

© 2006 Published by Elsevier Ltd on behalf of Acta Materialia Inc.

Keywords: Grain boundary migration; Grain rotation; Boundary energy anisotropy; Molecular dynamics; Phase field

1. Introduction

The evolution of polycrystalline microstructures is commonly described in terms of grain boundary migration. However, such microstructures can, in principle, also evolve by grain rotation. Since the excess energy of a polycrystalline body is the product of the grain boundary area and the grain boundary energy, either motion of the boundary to reduce its area (curvature-driven boundary migration) or grain rotation (assuming non-uniform boundary energies) can reduce the energy of the system. In fact, there have been several experimental observations of grain rotation, and microstructure evolution theories based upon grain rotation have been proposed. In the pres-

ent paper, we report the results of a series of molecular dynamics (MD) simulations of the evolution of a circular grain embedded within a large grain in which we observe simultaneous grain boundary migration and grain rotation.

The existence of grain rotation during microstructural evolution was first reported from observations of subgrain growth, which resulted in grain coalescence [1–4]. Li formulated the rate of grain rotation in terms of a dislocation model in which the interdislocation spacing evolved via non-conservative dislocation motion, resulting in the elimination of the boundary [5]. This analysis was based upon the Read–Shockley model for the dependence of grain boundary energy upon misorientation at low angles. This model was extended to include the removal of dislocations from a low-angle or subgrain boundary as a result of unbalanced forces associated with boundary terminations (i.e., triple junctions) [6,7]. Additional experimental

* Corresponding author. Tel.: +1 3032733683; fax: +1 3032733602.

E-mail address: mupmanyu@mines.edu (M. Upmanyu).

observations of subgrain coarsening in Al–0.46 wt.% Cu revealed that while boundaries seldom completely disappeared due to rotation, dislocation emission from very low-angle boundaries (i.e., misorientation $\theta < 0.3^\circ$) did occur [8].

Shewmon [9] proposed a grain rotation model to explain the experimental observations of Pond and Smith [10], in which rotation was controlled by the climb and/or glide of grain boundary dislocations (GBDs). The rate of these dislocation processes was described in terms of both volume and boundary diffusion. This analysis predicted an experimentally measurable rotation rate for spherical particles on a flat surface. Several experimental studies of the rotation of spherical single-crystal particles on single-crystal substrates were performed [11,12]. In the experiments of Erb and Gleiter [12], X-ray pole figures showed that Cu spheres on a (110) Cu plate rotated toward low-energy misorientations. Interestingly, the pole figure exhibited a large number of small-intensity peaks at low temperature, and a smaller number of more intense peaks upon annealing at high temperature. This suggests that at higher temperatures some of the minima in boundary energy versus misorientation are not deep enough to trap the rotating crystals at misorientations seen at low temperature [13]. While X-ray texture measurements cannot be used to determine the role of GBDs in rotation, dislocation motion during grain rotation was observed in transmission electron microscopy (TEM) studies. In their classic TEM studies of gold particle rotation, Chan and Balluffi reported the motion of screw dislocations (within the grain boundary and toward the free surface) during particle rotation toward low-angle and $\Sigma 5$ boundaries [14,15].

While the rotating particle experiments provide unequivocal examples of grain rotation, they represent a special case in which a grain is largely unconstrained (i.e., only a small fraction of the particle periphery corresponds to grain boundaries). On the other hand, in bulk materials (and thin films) grains are surrounded by other grains and, hence, are highly constrained. King and co-workers reported TEM observations of grain rotation in the vicinity of a propagating crack front during the annealing of thin, fine-grained, columnar, $\langle 111 \rangle$ textured gold films [16,17]. They observed correlated rotations of several grains, without the motion of other defects in the interior of the grains. This suggests the possibility of rigid body rotations of constrained grains. Randle observed a phenomenon, referred to as “grain boundary recovery”, in which a microstructure of pinned grain boundaries relaxes by grain rotation [18–23].

Most of the earlier analyses of grain rotation are based on Li’s theory of rotation via the motion/rearrangement of GBDs [5]. For example, Shewmon [9] and Erb [12] suggested that the rotation rate is proportional to the torque $\partial\gamma_{\text{gb}}/\partial\theta$, which for low-angle boundaries may be described in terms of the Read–Shockley relation [24]

$$\frac{\partial\gamma_{\text{gb}}}{\partial\theta} = -\gamma_o \ln\left(\frac{\theta}{\theta_m}\right) \quad (1)$$

where γ_o and θ_m are constants. This result suggests that the torque (and hence the rotation rate) diverges as the misorientation goes to zero. This approach neglects the possibility that the rotational mobility (i.e., the proportionality factor between torque and rotation rate) may vary with misorientation. This approach also does not necessarily reduce the total excess free energy due to the surface, which is the product of the surface energy and the surface area. Using a description based upon viscous motion of GBDs, Martin showed that the rotation rate decays algebraically with decreasing misorientation, thereby offsetting the logarithmic divergence in the torque [25]. Cahn analyzed the effect of the image forces on the GBDs associated with the presence of the free surface, suggesting a decrease in rotation rate with decreasing misorientation [26]. King and co-workers [17], using a Monte Carlo simulation approach, came to similar conclusions. The thermally activated motion of GBDs yields rotation rates that are consistent with experiment [27]. Quite recently Cahn and Taylor have investigated the necessary interaction between grain boundary motion and rotation, based solely on geometric relationships and physically imposed couplings between tangential and normal interface motion (during the submission and review cycle for this paper, a relevant manuscript by Cahn and Taylor has been published, and we are aware that another is in progress. A reconciliation of our atomistic and continuum models with their sharp interface model is worthy of further research.).

More recently, atomistic simulations of grain growth in polycrystals with nanoscale grains showed that both grain rotation and grain boundary migration occur during grain growth [28]. Based upon these observations, Moldovan et al. [29] developed a theory for grain rotation (using Raj and Ashby’s analysis of diffusively accommodated grain boundary sliding [30]), and developed a stochastic simulation approach based upon this rotational theory [31]. They concluded that the grain rotation rate scales with grain size as $1/R^5$. Recently, Kobayashi et al. introduced a microstructural model within the phase field framework that accounts for simultaneous grain boundary migration and grain rotation. This model employs one order parameter to describe the degree of local order (high in grains and low at grain boundaries) and one to describe the grain orientation [32]. Simulations using this approach are computationally intensive and the parameter space is large. Therefore, this model has yet to be fully explored and exploited.

In this study, we present atomistic and phase field simulation studies of simultaneous grain boundary migration and grain rotation for circular grains embedded in otherwise single-crystal matrices. Grain boundary curvature drives the migration (shrinkage) of the circular grain. The unconstrained circular shape of the grain facilitates its rotation. The simplicity of this grain rotation/boundary migration geometry is reflected in the small number of

variables needed to describe the evolution of the system: namely grain size and grain orientation. This facilitates easy extraction of the fundamental mobilities associated with both grain rotation and migration. These parameters represent the fundamental atomistic input to the phase field model for microstructural evolution. These input parameters are used within the sharp interface limit of the phase field model to examine the interdependence and competition between grain rotation and grain boundary migration. Comparisons of the predictions with MD results are used to validate the theoretical approach.

We first describe the atomistic simulation method, present the rotation and migration rates as a function of grain misorientation, and provide a preliminary analysis of the observations. Next, we describe a phase field model for coupled grain rotation and grain boundary migration in the sharp interface limit and apply it to the circular grain geometry of the MD simulations with mobility parameters determined from the MD simulations. We show excellent correspondence between the phase field and the atomistic simulation results. Based upon the atomistic and phase field simulations results, we discuss the mechanisms for grain rotation and the implications of grain rotation on grain growth.

2. Atomistic simulation method

The simulations were performed in two dimensions using a standard MD simulation method with a simple, empirical (Lennard-Jones) pair potential. This interatomic potential was chosen because it is both simple and well characterized rather than providing an accurate picture of any particular material. The simulations were performed in two, rather than three dimensions, in order to more clearly identify the rotation mechanism and for the sake of the computational efficiency necessary to examine a wide range of cases in relatively large systems. For more details on the MD simulation technique, see Ref. [33]. The simulation geometry used in this study (see Fig. 1(a)) consists of a circular grain embedded within another grain and is constrained to lie entirely in the XY -plane. The edges of the computational box represent free surfaces in order to allow the simulation cell to contract when the grain boundary area (length) decreases since there is a positive excess volume per unit area of grain boundary [34]. The interaction of the free surfaces with the circular grain boundary is kept to a minimum by ensuring that the closest approach of the grain boundary to any surface is greater than or equal to the initial radius of the circular grain, $R(0)$. Prior to the actual simulation, the as-constructed circular grain geometry is relaxed at a very low temperature ($0.010 \epsilon_{LJ}/k_B - 0.025 \epsilon_{LJ}/k_B$, where ϵ_{LJ} is the Lennard-Jones potential well depth and k_B is the Boltzmann constant). The entire system is then raised to the desired temperature using a thermostat [33].

The temporal evolution of the area of the circular grain $A(t)$ provides a measure of the boundary migration rate. $A(t)$ is simply the product of the number of atoms within the circular grain (see Ref. [33] for a description of the algo-

rithm used to identify in which grain each atom lies) and the area per atom at the temperature of interest, a_o . The slope of the A versus simulation time plot is the instantaneous rate of shrinkage of the circular grain. The time dependence of the grain orientation provides a measure of the grain rotation rate. The simulations are performed for initial misorientations within the range $30^\circ < \theta(t=0) < 48^\circ$ and at a temperature $T = 0.125 \epsilon_{LJ}/k_B$.

We analyze the grain rotation rate in terms of the misorientation dependence of the grain boundary energy (enthalpy) γ_{gb} . The grain boundary energy (averaged over all boundary inclinations) versus misorientation for the same interatomic potential, lattice and temperature used here was determined in Refs. [35,36]. The energies are reported in units of ϵ_{LJ} , distance in units of the equilibrium atom separation r_o , area in units of the perfect crystal area per atom a_o and time in units of $\tau = \sqrt{M_{at} r_o^2 / \epsilon_{LJ}}$, where M_{at} is the atomic mass. For example, in the case of Al, $\epsilon_{LJ} = 0.57$ eV, $r_o = 2.86$ Å and $\tau = 0.2$ ps.

3. Atomistic simulation results

Fig. 1(a)–(f) show the atomic configurations within the computational cell for $\theta(0\tau) = 34^\circ$, $T = 0.125 \epsilon_{LJ}/k_B$ and $A(0\tau) = 2400 a_o$. The atomic configurations correspond to time steps $t = 0, 320, 570, 940, 1370$ and 1740τ . Apart from thermal fluctuations, the embedded grain remains circular while it shrinks. Marker lines are drawn along close-packed (i.e., instantaneous $\langle 11 \rangle$) directions within the shrinking grain for a visual confirmation of the grain orientation and rotation (see Fig. 1(a)–(f)). Superposition of the marker lines at various simulation times (inset in Fig. 1(f)) confirms a net change in the misorientation across the grain boundary. Following an initially rapid change in grain orientation, the grain appears to shrink at nearly constant orientation (see Fig. 1(d)–(f)). Eventually, the initially circular grain disappears completely, leaving behind a vacancy cluster, which accounts for the excess volume associated with the grain boundary not elastically transferred to the free surfaces.

Fig. 2 shows the temporal variation of the misorientation and area of the shrinking grain for the simulations shown in Fig. 1, averaged over a time of 5τ and three independent simulation runs. Significant rotation is observed for the time interval $t \leq 1200\tau$, during which the misorientation across the grain boundary changes from $\theta(0\tau) = 34^\circ$ to $\theta(1200\tau) \cong 39^\circ$. For $t \geq 1200\tau$, there is little further rotation of the circular grain and the misorientation settles down to $38.2^\circ \pm 0.3^\circ$. For $t \geq 1600\tau$, the small grain size ($< 7r_o$) makes it difficult to extract meaningful grain orientation statistics (see Fig. 1(f)) and, hence, the grain evolution is ignored at these times. If the grain boundary surface tension remained constant as the grain shrank, we should expect that A would decrease linearly with time. However, contrary to expectations, Fig. 2 demonstrates that in this particular case, A decreases with time more slowly.

Fig. 3 shows the temporal evolution of the atomic configurations for a grain with initial misorientation $\theta(0) = 42^\circ$ at three different times ($t = 25, 700$ and 1200τ). As in the

$\theta(0) = 34^\circ$ case, the grain remains nearly circular as it shrinks. Examination of the changes in the orientations of the lines marking the close-packed direction (Fig. 3(c))

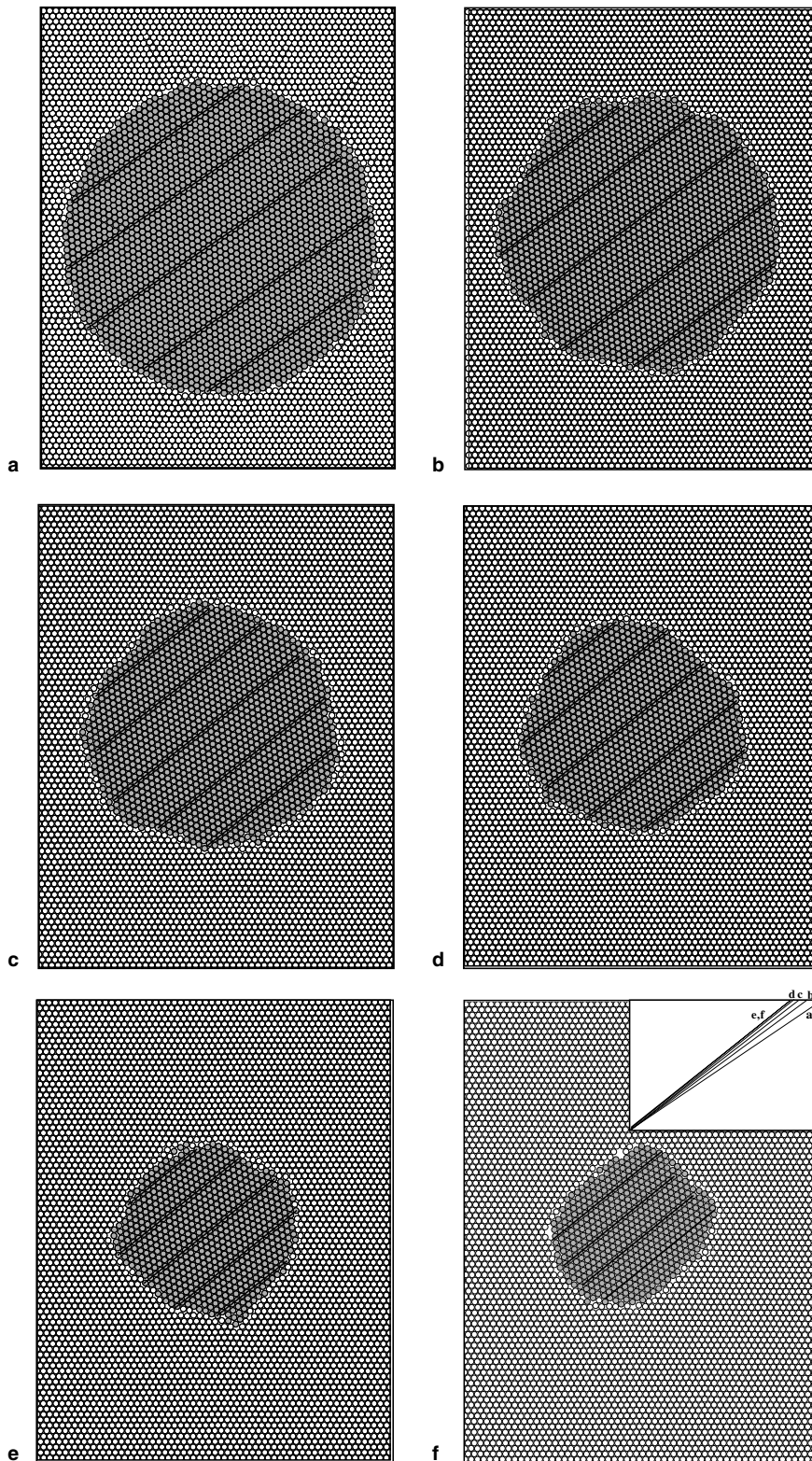


Fig. 1. Atomic position in the circular grain bicrystal at simulation times: (a) 0; (b) 320τ ; (c) 570τ ; (d) 940τ ; (e) 1370τ ; (f) 1740τ for a grain of initial area $2100a_0$ at $T = 0.125\varepsilon_{LJ}/k_B$. The initial misorientation between the two grains is $\theta(0) = 34^\circ$. The straight lines indicate a particular close-packed direction within the circular grain. The change in the slope of these lines indicates the degree to which the initially circular grain has rotated. The orientations of these lines for the six different times shown are tabulated in the upper right corner of (f).

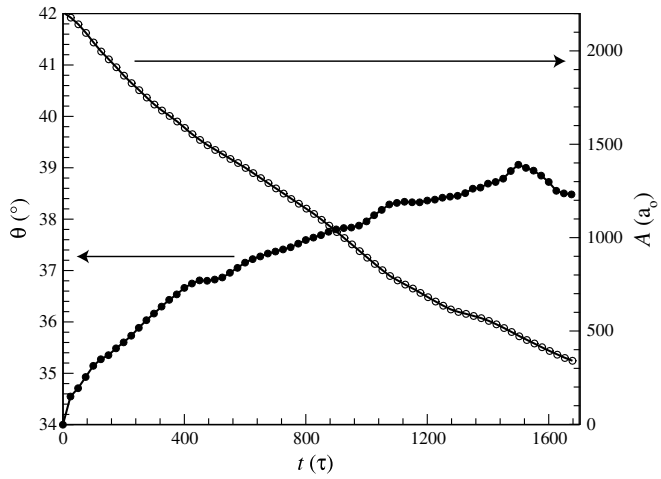


Fig. 2. Temporal evolution of the misorientation and area of the initially circular grain for the same conditions as for Fig. 1. The data were averaged over a time of 5τ and three independent simulation runs.

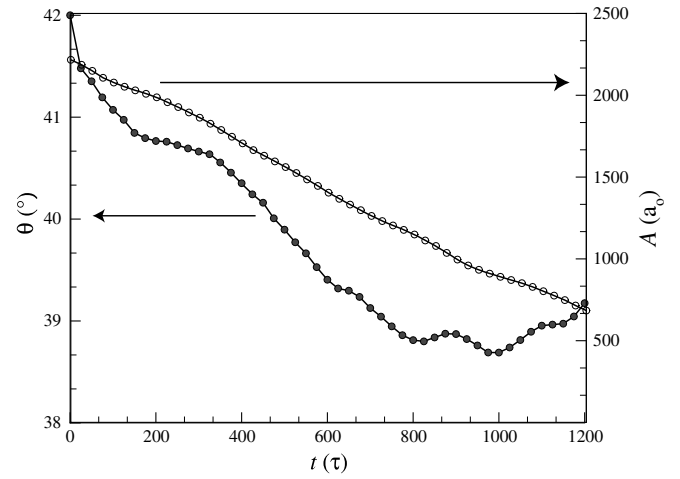


Fig. 4. Temporal evolution of the misorientation and area of the initially circular grain for the same conditions as for Fig. 3. The data were averaged over a time of 5τ and three independent simulation runs.

demonstrates that some grain rotation occurs. However, compared with the $\theta(0) = 34^\circ$ case (Fig. 1), the magnitude of the rotation is smaller and the sign of the rotation has

switched. Fig. 4 shows the variation of this angle and the grain size with time. The misorientation decreases for times $0 \leq t \leq 750\tau$ and then oscillates about a value of

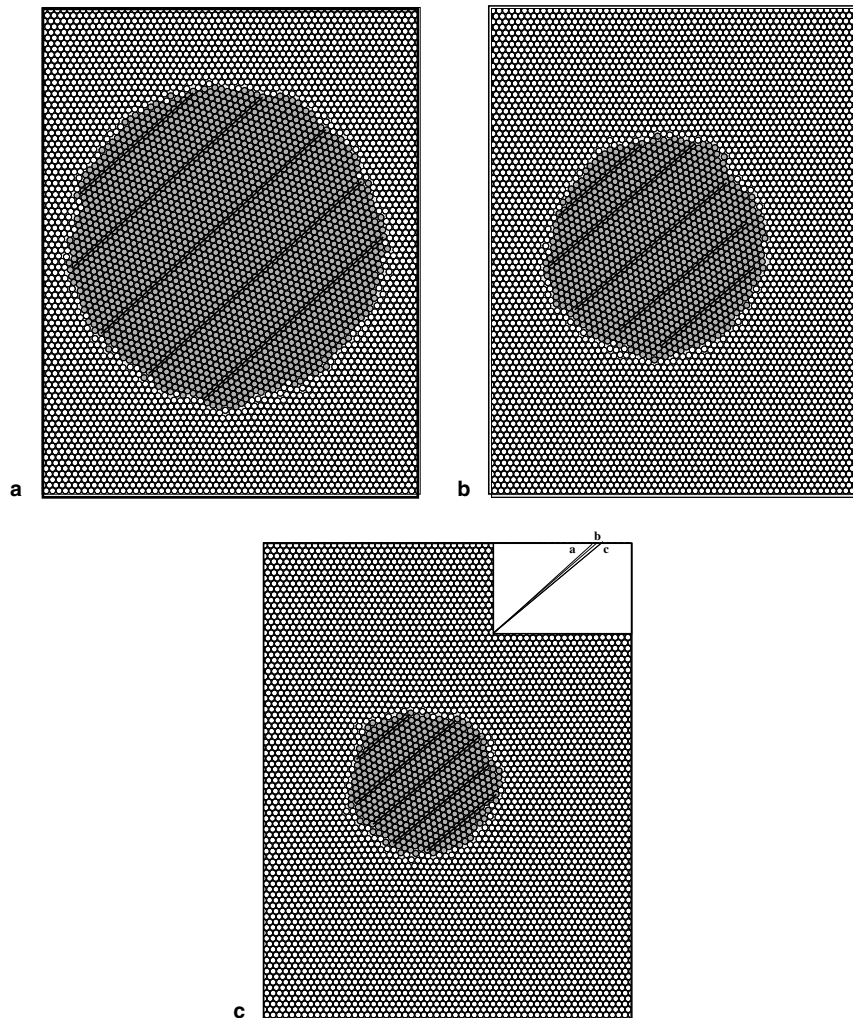


Fig. 3. As per Fig. 1, but for the case of an initial misorientation of $\theta(0) = 42^\circ$: (a) 25τ ; (b) 700τ ; (c) 1200τ .

$38.2^\circ \pm 0.3^\circ$. The variation of the orientation with time is not smooth. Although the variation of grain area with time is much more linear in the present case than for $\theta(0) = 34^\circ$, we see a correlation between non-uniformities in the rotation and shrinkage rates.

In the two simulations described above, the embedded grain rotates to a final misorientation that lies between 38° and 39° . A misorientation of $\theta = 38.2^\circ$ corresponds to the high-symmetry grain boundary $\Sigma = 7$. In order to determine whether a grain with a boundary that initially has this special misorientation is stable with respect to rotation, simulations were performed for this misorientation. Fig. 5 shows the temporal evolution of the atomic structure of a shrinking, initially circular grain with a $\theta(0) = 38.2^\circ$, $\Sigma = 7$ grain boundary. As for the cases examined above, the shrinking grain remains nearly circular. However, the inset in Fig. 5(c) demonstrates that there is almost no change in misorientation as the initially circular grain shrinks. The variation of the misorientation and area of the shrinking grain with time is shown in Fig. 6. While the rate of change of area of the circular grain is nearly lin-

ear, there is little or no variation in the misorientation across the grain boundary (i.e., significant grain rotation does not occur). The simulation results suggest that for initial misorientations in the $34\text{--}42^\circ$ range, the grain always rotates toward $\Sigma = 7 - \theta = 38.2^\circ$. This high-symmetry misorientation is a fixed point for grain rotation.

In order to determine if other high-symmetry, low- Σ boundaries are likewise fixed points for rotations, a series of simulations were performed for 13 different initial misorientations, i.e., $30^\circ \leq \theta(0) \leq 48^\circ$. Three high-symmetry, low- Σ misorientations exist in this high-angle misorientation regime: $\Sigma = 19 - \theta = 46.8^\circ$, $\Sigma = 7 - \theta = 38.2^\circ$ and $\Sigma = 13 - \theta = 32.2^\circ$ [37] (see Fig. 7). Figs. 8 and 9 show the evolution of the average misorientation for the $\theta(0\tau) = 32^\circ$ (i.e., near the $\Sigma = 13 - \theta = 32.2^\circ$ misorientation) and $\theta(0\tau) = 48^\circ$ (i.e., near the $\Sigma = 19 - \theta = 46.8^\circ$ misorientation) grain boundaries, respectively. In the former case, grain rotation occurs such that the misorientation across the grain boundary continuously increases and asymptotes at a value that corresponds to the $\Sigma = 7$ boundary, i.e., $\theta(t \geq 1500\tau) \cong 38.2^\circ$. Similar behavior is observed

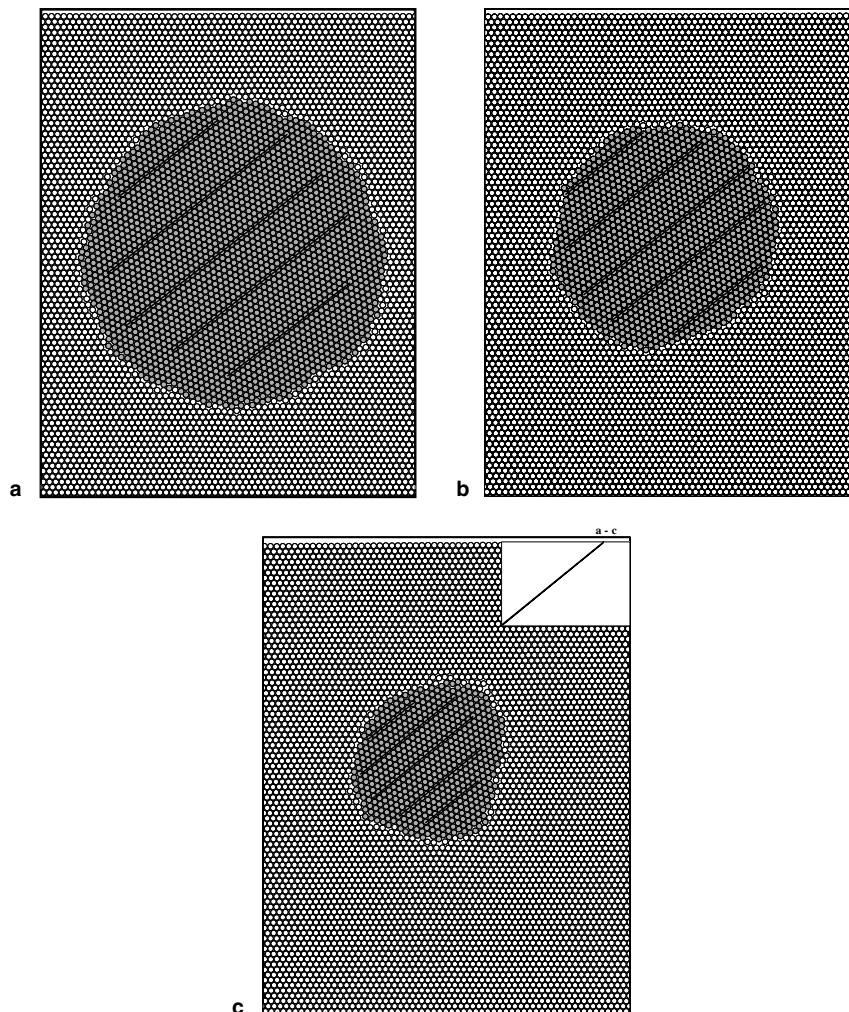


Fig. 5. As per Fig. 1, but for the case of an initial misorientation of $\theta(0) = 38.2^\circ$: (a) 25τ ; (b) 650τ ; (c) 1170τ .

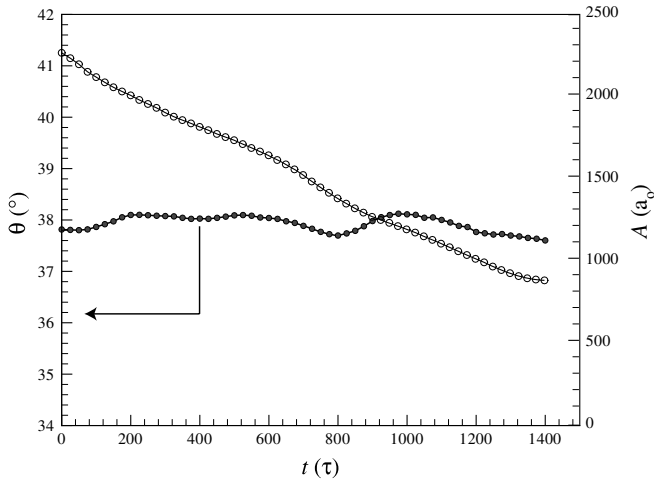


Fig. 6. Temporal evolution of the misorientation and area of the initially circular grain for the same conditions as for Fig. 5.

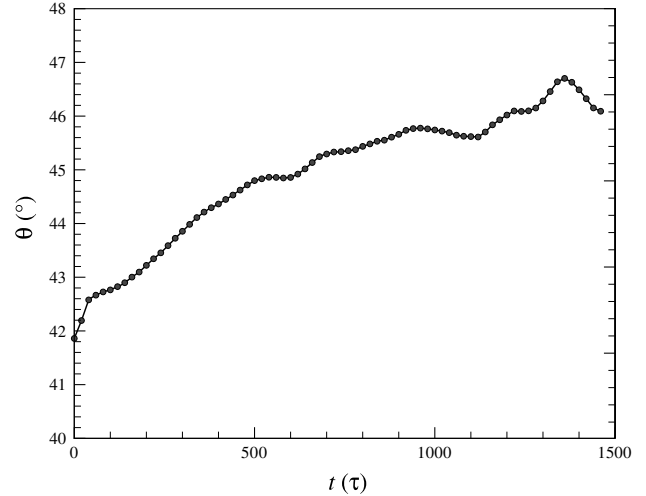


Fig. 9. Temporal evolution of the misorientation of the initially circular grain for $\theta(0) = 42^\circ$.

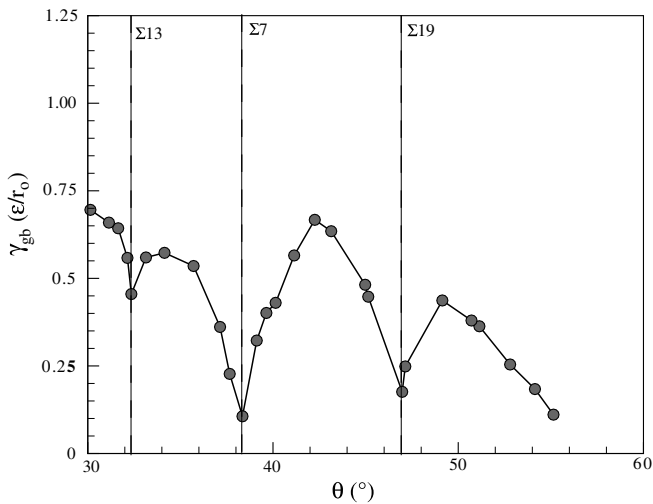


Fig. 7. Variation of the grain boundary internal energy γ_{gb} with boundary misorientation, extracted from bicrystal simulations of half-loop boundary geometries in a two-dimensional Lennard-Jones system [36].

for a grain with an initial misorientation corresponding to the $\Sigma = 13$ boundary (i.e., $\theta(0\tau) = 32.2^\circ$) and also for $\theta(0\tau) = 30^\circ$ (both not shown). This implies that, unlike the $\Sigma = 7$ grain boundary, the high-symmetry $\Sigma = 13$ boundary does not correspond to a fixed point for grain rotation. For the $\theta(0\tau) = 48^\circ$ simulation, the grain once again rotates, but in this case to the neighboring high-symmetry $\Sigma = 19$ ($\theta = 46.8^\circ$) misorientation. This rotation behavior is observed for all initial misorientations within the range $44^\circ \leq \theta(0) \leq 48^\circ$, implying that the misorientation corresponding to the $\Sigma = 19$ boundary is a fixed point for grain rotation as well.

The initial and final grain misorientations found in the circular grain simulations for the 13 different misorientations examined are shown in Table 1. The data reported are averaged over 3 independent simulation runs for $T = 0.125\epsilon_{LJ}/k_B$ and $A(0) = 1200a_0$. Our results show that grain rotation always occurs during grain boundary migration except for a few, high-symmetry misorientations (at least for the initially circular grains considered here). For the range of initial misorientations examined, rotation

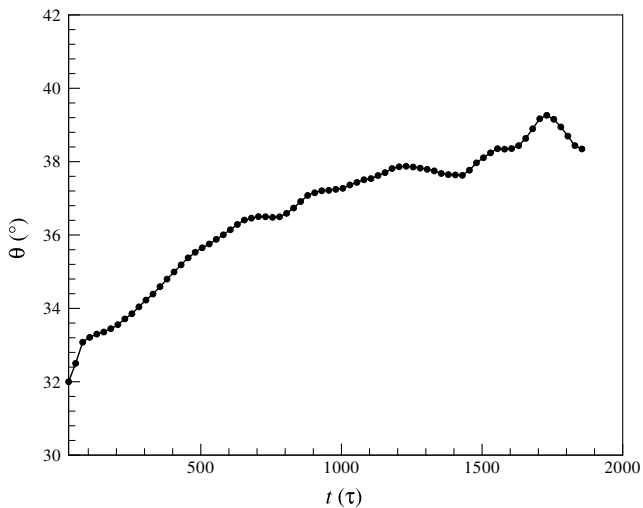


Fig. 8. Temporal evolution of the misorientation of the initially circular grain for $\theta(0) = 32^\circ$.

| $\theta(0)$ ($^\circ$) | θ_f ($^\circ$) |
|--------------------------|-------------------------|
| 30 | 38.5 ± 0.5 |
| 32 | 38.3 ± 0.4 |
| 32.2– $\Sigma 13$ | 38.2 ± 0.3 |
| 34 | 38.2 ± 0.3 |
| 36 | 38.3 ± 0.3 |
| 38 | 38.2 ± 0.3 |
| 38.2– $\Sigma 7$ | No rotation |
| 40 | 38.2 ± 0.3 |
| 42 | 38.2 ± 0.3 |
| 44 | 47 ± 1 |
| 46 | 47 ± 1 |
| 46.8– $\Sigma 19$ | No rotation |
| 48 | 46 ± 0.5 |

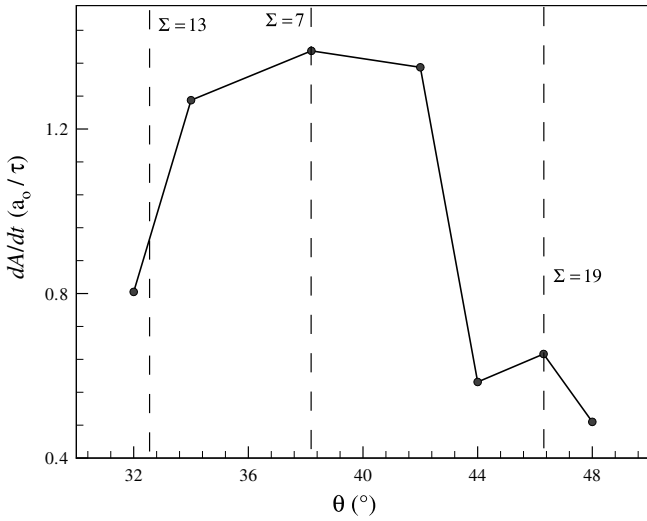


Fig. 10. The rate of change of the grain area $(dA/dt)|_A$ versus misorientation θ at fixed grain size, $A = A(0) = 2400a_0$.

occurs toward either the high-symmetry $\Sigma = 7$ or $\Sigma = 19$ misorientations. Simulations with initial misorientations corresponding to these two special values do not rotate

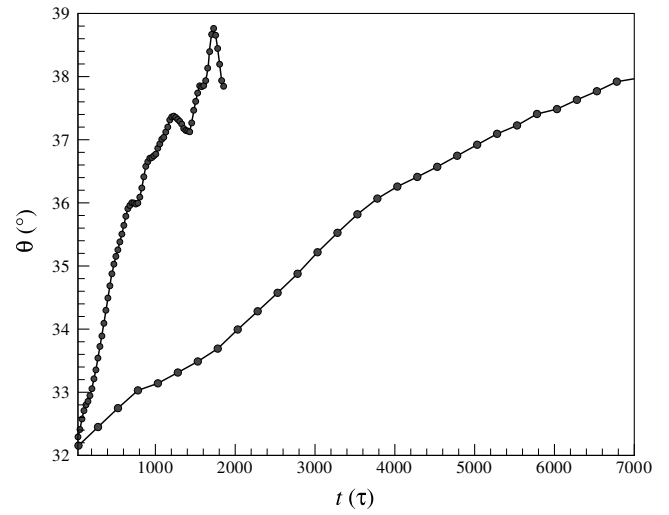


Fig. 11. Temporal evolution of the misorientation of two initially circular grains with $\theta(0) = 32^\circ$ and $A(0) = 2400a_0$ and $9600a_0$.

during grain boundary migration. Surprisingly, although the $\Sigma = 13$ misorientation corresponds to a high-symmetry situation, grains with this misorientation rotate away and

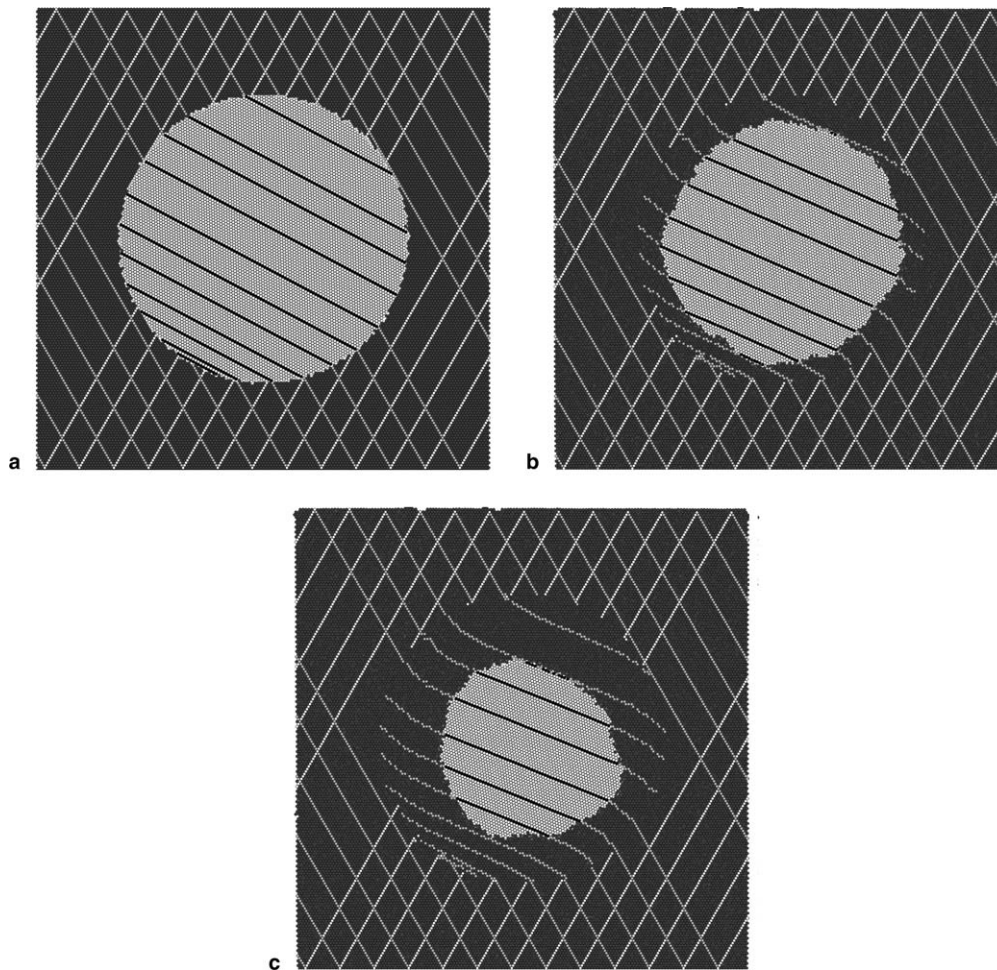


Fig. 12. Atomic position in the circular grain bicrystal at simulation times: (a) 0; (b) 1031τ ; (c) 2031τ for a grain of initial area $9600a_0$ at $T = 0.125\varepsilon_{LJ}/k_B$. Several lines of atoms along close-packed directions are colored differently from their surroundings in order to have a history of atomic positions during grain boundary migration/rotation and to identify slip steps.

other grains rotate through this misorientation. Therefore, while the $\Sigma = 7$ and $\Sigma = 19$ are fixed points for rotation, not all Σ misorientations correspond to fixed points.

We now examine the interplay between grain rotation and grain boundary migration by examining $(dA/dt)|_{A=A_0}$ for different misorientations and $(d\theta/dt)|_{\theta=\theta_0}$ for different grain sizes, where A_0 and θ_0 are reference grain area and misorientation, respectively. Fig. 10 shows $(dA/dt)|_{A=A_0}$ versus θ from the data reported above, evaluated for the same initial grain size $A_0 = A(0\tau)$. The data show that there are maxima in the grain boundary migration rates at the high-symmetry, low- Σ boundaries, $\Sigma = 7$ and $\Sigma = 19$, but not near $\Sigma = 13$. This observation correlates with the observation that the $\Sigma = 7$ and $\Sigma = 19$ misorientations represent fixed points for grain rotation, while the $\Sigma = 13$ misorientation is not. These data are consistent with the MD simulation results in the half-loop geometry performed at the same temperature [35], which show that grain boundaries with misorientations corresponding to $\Sigma = 7$, $\Sigma = 13$ and $\Sigma = 19$ all represent local maxima in plots of the reduced mobility (i.e., product of the grain boundary mobility and grain boundary energy) versus misorientation. No rotation was possible in those simulations. Our results clearly elucidate the connection between the grain rotation process and grain boundary migration.

Fig. 11 shows misorientation versus time for two grains at the same misorientation but with different grain sizes. Clearly, the rate of change of the orientation varies dramatically with grain size. There have been many and varied predictions on how the rotation rate depends on grain size, all of which can be described by a power law of the form $(d\theta/dt) \propto R^{-n}$, where n is variously 0, 2, 3, 4 or 5 depending on the rotation mechanism assumed in the theory [5,9,17,25–27,30]. If we extract values of the rate of change of the orientation at the beginning of the simulation $(d\theta/dt)|_{\theta=\theta(0\tau)}$ from Fig. 11 and fit the results to the form $(d\theta/dt) \propto R^{-n}$, we find $n = 2.6 \pm 0.5$. Given the magnitude of the uncertainty, this is consistent with models that predict either $n = 2$ [38] or $n = 3$ [9].

The different models for the dependence of rotation rate on grain size are based upon different assumptions regarding the grain rotation mechanism, as discussed in Section 1. There are fundamentally just two types of models: (i) rigid rotation models, in which the grain rotates because of processes occurring near or at the grain boundaries, such as primary or secondary grain boundary dislocation climb (the rate of rotation depends on the transport mechanism that produces climb) and (ii) grain shearing models, in which dislocations glide across the grains. In order to determine whether rotation actually occurs in accordance with the second model, we look for evidence of slip in the grain interior. We do this by identifying lines of atoms along the close-packed directions and observe whether any of these lines exhibit slip steps following rotation. Fig. 12 shows the results of such a study for the case of a large grain with an initial orientation of $\theta(0\tau) = 32^\circ$. If a dislocation traversed a grain and crossed one of the shaded lines

of atoms, such a line would show a step of one atomic height. Examination of this series of figures shows that grain rotation occurs in a nearly rigid body type of motion and that slip steps are not formed within the grain interior. These observations suggest that a rigid rotation mechanism is operative, as earlier theories suggest.

4. Phase field model

Recently, Kobayashi, Warren and Carter (KWC) introduced a model of grain boundaries [32] based on earlier work by the same authors [39,40]. The choice of the free energy in this model was motivated by the requirement that the physical properties of the solutions remained invariant under rotation of the frame of reference. It employed the phase field formalism, which proved to be remarkably successful for modeling solidification.

For a chemically pure solid with no liquid phase, the KWC order parameters η and θ represent a coarse-grained measure of the degree of crystalline order and the crystalline orientation, respectively. The following describes one approach for defining these order parameters by coarse graining an approximate microscopic variable. In a mesoscopic region, which is large compared to the bond length but still small compared to the dimensions of a grain, we define η and θ as an average over such regions:

$$\langle e^{in\theta_i} \rangle = \eta e^{in\theta} \quad (2)$$

where n is the order of the rotational symmetry. The local orientation variable $\theta(\mathbf{x},t)$ varies between 0 and $2\pi/n$. The degree of orientational order $\eta(\mathbf{x},t)$ lies between 0 and 1: $\eta = 1$ reflects a completely oriented state, while $\eta = 0$ a state where no meaningful orientation order exists. Grain boundaries are characterized by a minimum in η and $\nabla\theta \neq 0$, while orientation is constant for grain interiors, i.e., $\nabla\theta = 0$. While this averaging procedure motivates the use of the two order parameters, no attempt is made to correlate the spatiotemporal evolution of these parameters with atomic-scale events.

Given these order parameters, KWC constructed a free energy, developed equations of motion for the order parameters and studied them numerically. However, in order to make contact with the MD simulation as well as with real laboratory experiments, one needs to relate unfamiliar model parameters to measured values. There are two available methods to achieve such comparisons. The first is direct numerical experiments, which is a difficult task since the parameter space is large and computation is intensive. A small number of such experiments were done by KWC [39,40].

The second approach, which is more common for phase field models, is to determine the behavior of the system *analytically* in the limit that the grain boundary is thin compared to all other length scales in the microstructure. This justifies comparisons with classic sharp interface theories. Lobkovsky and Warren [38] determined the surface

energy, grain boundary mobility and rotation rates for a generalized version of the KWC model as a function of model parameters in the sharp interface limit. We refer to this extended version of KWC as KWCL.

Much of what is described below can be found in Ref. [38]. In the KWCL model, the free energy takes the following generalized form:

$$F[\eta, \theta] = \frac{1}{\varepsilon} \int_{\Omega} dA \left[\frac{\alpha^2}{2} |\nabla \eta|^2 + f(\eta) + g(\eta)s|\nabla \theta| + h(\eta) \frac{\varepsilon^2}{2} |\nabla \theta|^2 \right] \quad (3)$$

where α , ε and s are positive model parameters. The overall prefactor ensures that the grain boundary energy tends to a non-zero constant in the $\varepsilon \rightarrow 0$ limit. We choose $f(\eta)$ to be a single well with minimum at $\eta = 1$ and $f(1) = 0$. Couplings $g(\eta)$ and $h(\eta)$ must be monotonically increasing and $h(\eta)$ has to be positive. The gradient flow equations read formally

$$Q(\eta, \nabla \theta) \tau_{\eta} \frac{\partial \eta}{\partial t} = -\varepsilon \frac{\delta F}{\delta \eta} = \alpha^2 \nabla^2 \eta - f_{\eta} - g_{\eta} s |\nabla \theta| - h_{\eta} \frac{\varepsilon^2}{2} |\nabla \theta|^2 \quad (4a)$$

$$P(\eta, \nabla \theta) \tau_{\theta} \eta^2 \frac{\partial \theta}{\partial t} = -\varepsilon \frac{\delta F}{\delta \theta} = \nabla \cdot \left[h \varepsilon^2 \nabla \theta + g s \frac{\nabla \theta}{|\nabla \theta|} \right] \quad (4b)$$

where we used the subscript to denote differentiation. The mobility functions P and Q must be positive definite and continuous at $\nabla \theta = 0$, but are otherwise unrestricted.

In the sharp interface limit $\varepsilon \rightarrow 0$, we choose the scaling of the model parameters to be

$$\alpha = \varepsilon \tilde{\alpha}, \quad s = \varepsilon \tilde{s}, \quad \tau_{\eta} = \varepsilon^2 \tilde{\tau}_{\eta}, \quad \tau_{\theta} = \varepsilon^2 \tilde{\tau}_{\theta} \quad (5)$$

Taking this limit allows us to predict the grain boundary profile, along with its energy and mobility. The values of the order parameter at the edge η_{\min} and at the center η_{\max} of the grain boundary can be found from the following two equations [38]:

$$g(\eta_{\max}) = g(\eta_{\min}) + \frac{\sqrt{2f(\eta_{\min})h(\eta_{\min})}}{\tilde{s}} \quad (6)$$

$$|\Delta \theta| = 2\tilde{\alpha} \tilde{s} \int_{\eta_{\min}}^{\eta_{\max}} d\eta \frac{g(\eta_{\max}) - g}{h \sqrt{2f - \frac{\tilde{s}^2 (g(\eta_{\max}) - g)^2}{h}}} \quad (7)$$

where $\Delta \theta$ is the jump in orientation across the grain boundary. Given η_{\min} and η_{\max} , we can determine the grain boundary energy [38]

$$\gamma = \tilde{s} g(\eta_{\max}) |\Delta \theta| + 2\tilde{\alpha} \int_{\eta_{\min}}^{\eta_{\max}} d\eta \sqrt{2f} + 2\tilde{\alpha} \int_{\eta_{\max}}^{\eta_{\min}} d\eta \sqrt{2f - \frac{\tilde{s}^2 (g(\eta_{\max}) - g)^2}{h}} \quad (8)$$

The normal velocity of the grain boundary is proportional to its curvature κ and energy γ

$$v = -M\kappa\gamma \quad (9)$$

where the grain boundary mobility M is given by [38]

$$\frac{1}{M} = \frac{\tilde{\tau}_{\eta}}{\tilde{\alpha}} \int_{\eta_{\min}}^{\eta_{\max}} Q d\eta \sqrt{2f - \frac{\tilde{s}^2 (g(\eta_{\max}) - g)^2}{h}} + \frac{\tilde{\tau}_{\eta}}{\tilde{\alpha}} \int_{\eta_{\min}}^{\eta_{\max}} Q d\eta \sqrt{2f} + \tilde{\tau}_{\theta} (\tilde{\alpha} \tilde{s})^2 \int_{\eta_{\min}}^{\eta_{\max}} P d\eta \frac{\eta^2 (g(\eta_{\max}) - g)^2}{h^2 \sqrt{2f - \frac{\tilde{s}^2 (g(\eta_{\max}) - g)^2}{h}}} \quad (10)$$

The rotation rate of a single, isolated grain of area A and perimeter length L embedded in an otherwise single-crystal matrix, $\partial \theta / \partial t$ is

$$\frac{\partial \theta}{\partial t} = \frac{\tilde{s}}{\varepsilon \tilde{\tau}_{\theta}} \frac{L g(\eta_{\max})}{\int_A dA \eta^2 P(\eta, 0)} \quad (11)$$

5. Phase field results

We can obtain and solve the equations describing the evolution of a circular grain in a matrix explicitly (a single integral for each quantity of interest). Additionally, we can use fits to the simulation results to extract realistic values of the parameters in this model and determine to what degree the KWCL model is capable of reproducing the trends in the simulation results. The MD results show that the embedded grains tend to rotate to special misorientations corresponding to cusps in the grain boundary energy. Therefore, integrating the MD results requires a meaningful way to define special misorientations within the phase field method. Since the order parameter η must be non-negative, we can define a high-symmetry grain boundary with misorientation θ_s as a sub-region where $\eta_{\min} = 0$. To model a circular grain of area A and orientation θ embedded in an otherwise single-crystal matrix (orientation $\theta = 0^\circ$), and its rotation towards the special misorientation θ_s , we choose $Q = 1$, $P = -\ln(1 - \eta)$, $f = \frac{1}{2}(1 - \eta)^2$, $g = \eta^2 - \mu$ and $h = \eta^2$. Shifting $g(0)$ down by μ creates a cusp in the grain boundary energy at the special misorientation θ_s . The logarithmically divergent P ensures a finite rotation rate in the sharp interface limit. We extract the grain boundary energy and mobility for the special grain boundary by taking the limit $\eta_{\min} \rightarrow 0$:

$$\gamma = \gamma_o + \mu \tilde{s} |\theta - \theta_s| + O((\theta - \theta_s)^2) \quad \text{and}$$

$$M = M_o + O((\theta - \theta_s)^2) \quad (12)$$

where $\theta_s = \tilde{\alpha} \pi$, $\gamma_o = \tilde{\alpha} (1 - \mu \tilde{s} \pi)$ and $M_o = 2\tilde{\alpha} / \tilde{\tau}_{\eta}$. By fitting the numerically measured grain boundary energy near the $\Sigma = 7$ boundary misorientation, we obtain $\mu \tilde{s} = 0.170 \pm 0.012$ and $\tilde{\alpha} = 0.271 \pm 0.026$. Using $v = -M\kappa\gamma$, we obtain

$$\dot{A} \approx -a_1 \quad (13)$$

where $a_1 = 2\pi \gamma_o M_o$. The rate of shrinking of a circular grain of instantaneous area A and misorientation θ can be obtained from Eq. (11):

$$\dot{\theta} \approx \frac{a_2}{A} \text{sign}(\theta_s - \theta) \quad (14)$$

where $a_2 = 6\pi\mu\tilde{\alpha}/\tilde{\tau}_\theta$ and sign is the signum function (i.e., -1 for $x < 0$, $+1$ for $x > 0$ and 0 for $x = 0$). Eqs. (13) and (14) are valid for misorientations near cusps in the grain boundary energy versus misorientation plot. However, they cannot be directly applied at $\theta = \theta_s$, where rotation rate diverges. Such divergences are an artifact of the sharp interface model. However, the presence of strong, sharp maxima in the migration rate at $\theta = \theta_s$ (e.g., for the $\Sigma = 7$ misorientation) have been observed in earlier MD simulations [35]. These equations can be easily solved for the evolution of grain area and orientation

$$A(t) = A(0) - a_1 t, \quad \theta(t) = \theta(0) - \text{sign}(\theta - \theta_s) \frac{a_1}{a_2} \log \frac{A(t)}{A(0)} \quad (15)$$

A fit to the MD grain area and misorientation versus time data near $\theta_s = 38.2^\circ$ (i.e., $\Sigma = 7$) yields $a_1 = 1.42 \pm 0.02$ and $a_2 = 0.183 \pm 0.005$. Using the expressions for a_1 and a_2 in terms of the phase field model parameters and the previously fitted values of $\mu\tilde{s}$ and $\tilde{\alpha}$, we obtain the two time constants $\tilde{\tau}_\eta = 4.12 \pm 0.38$ and $\tilde{\tau}_\theta = 4.74 \pm 0.41$.

Figs. 13 and 14 compare the KWCL predictions with the MD simulation results for the time dependence of the area and orientation of the circular grain for the case of $\theta(0\tau) = 32^\circ$ and $A(0\tau) = 2400a_o$ at $T = 0.125\epsilon_{LJ}/k_B$. Examination of these two plots shows excellent agreement between the MD and KWCL sharp interface results. Although the kinetic parameters in the KWCL model were extracted from the MD simulations, the fact that the KWCL predictions are in agreement with the MD data is an important result. This agreement is only possible because the functional forms of the KWCL model prediction are consistent with the physics of simultaneous grain boundary migration and grain rotation phenomena. The main result of the present analysis is that the rotation rate scales with the grain size R as $\dot{\theta} \propto R^{-2}$.

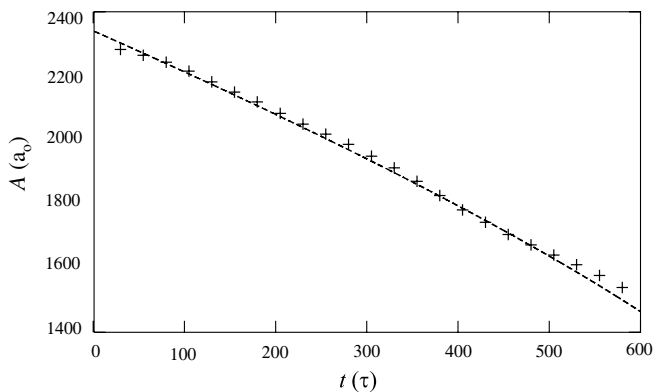


Fig. 13. Temporal evolution of the area of an initially circular grain with $\theta(0) = 32^\circ$ and $A(0) = 2400a_o$ at $T = 0.125\epsilon_{LJ}/k_B$. The + symbols represent MD simulations (averaged over a time of 5τ and three independent simulation runs) and the dashed line represents the phase field results (an integral of Eq. (13) where the parameter a_1 was determined by fitting to the simulation results, as described in the text).

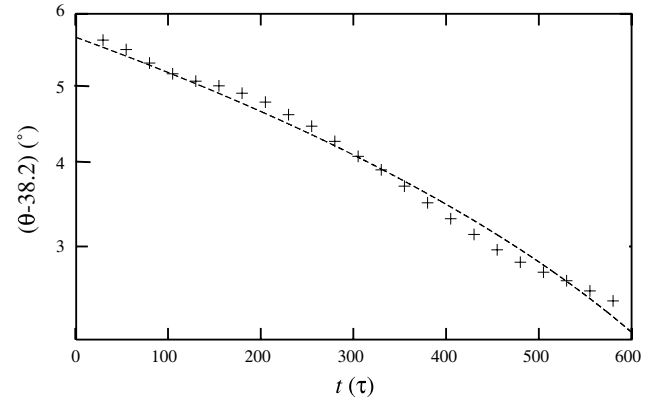


Fig. 14. Temporal evolution of the misorientation of the initially circular grain with $\theta(0) = 32^\circ$ and $A(0) = 2400a_o$ at $T = 0.125\epsilon_{LJ}/k_B$. The + symbols represent MD simulations (averaged over a time of 5τ and three independent simulation runs) and the dashed line represents the phase field results (an integral of Eq. (14) where the parameter a_2 was determined by fitting to the simulation results, as described in the text).

6. Discussion and conclusions

We have performed a series of MD simulations of shrinking circular grains. These simulations clearly demonstrate that grain boundary migration and grain rotation can occur simultaneously, especially at small grain sizes. For the nanoscale dimensions examined here, we commonly observe that grain rotation occurs at a sufficiently fast rate such that the grain orientation may saturate long before the grain disappears by grain boundary migration. In real polycrystals, on the other hand, grain rotation may be impeded by the presence of triple and quadruple junctions that commonly lead to manifestly non-spherical grains.

Grains tend to rotate in a direction that is consistent with the local gradient in the grain boundary energy (i.e., the torque, $\partial\gamma/\partial\theta$). In the present simulations, these local gradients led to grain rotation into high-symmetry, low- Σ orientations, where the boundary energy was a local minimum. In the misorientation range examined, two such special orientation fixed points were observed, corresponding to the $\Sigma = 7$ and $\Sigma = 19$ misorientations. Surprisingly, however, grains rotated past the orientation corresponding to $\Sigma = 13$. This orientation, however, corresponds to a relatively shallow minimum in the grain boundary internal energy and we have no assurance that this orientation is also a minimum in the grain boundary free energy. Therefore, it still may be appropriate to conclude that grain boundaries migrate in accordance with local torques.

In order to understand the trends observed in the MD simulations, we performed an analysis of simultaneous grain boundary migration and grain rotation within the phase field model framework, in the sharp interface limit. This model predicts that the grain shrinkage rate ($\partial A/\partial t$) is independent of both grain size and the misorientation (for misorientations close to those where there are cusps in the grain boundary energy versus misorientation plot). The independence of grain size neglects the *dynamic*

correlations between grain size, misorientation and grain boundary energy. This predicted independence of the shrinkage rate with respect to misorientation is consistent with the MD simulation results.

The phase field model also predicts that the rotation rate is proportional to the inverse square of the grain size, R , and is only dependent upon the sign of the misorientation. We extracted the power law dependence of the rotation rate on grain size from (admittedly sparse) MD data. These data suggest that the rotation rate is proportional to R^{-n} , where $n = 2.6 \pm 0.5$. This is consistent with the phase field model predictions. Note that both the phase field and MD prediction of $n \approx 2$ is smaller than the exponent predicted by most other grain rotation theories.

The relative rates of grain boundary migration and grain rotation dictate the degree to which grain rotation is important in grain growth processes. The results of the phase field simulations presented above (for misorientations near cusps) and the MD results suggest that the rotation rate scales with grain size as $\dot{\theta} \propto R^{-2}$ and the rate at which the grain size changes scales with grain size as $\dot{R} \propto R^{-1}$. Based on these different exponents, we should expect that as grain sizes increase, rotation becomes less important relative to boundary migration. However, to put these two quantities on the same footing, we should look at how these two processes affect the same system parameter. If we focus on the total energy of the system (i.e., the product of the grain boundary perimeter and the grain boundary energy, as per Eq. (12)) and assume that $\dot{\theta} \propto R^{-2}$ and $\dot{R} \propto R^{-1}$, we find that both the rotation and migration contributions to the energy scale as R^{-1} . Therefore, rotation makes just as important a contribution to the relaxation of the energy of the system at large grain sizes as it does at small sizes. Therefore, while the rate of grain rotation decreases faster with increasing grain size than does the migration rate, it may still be important at larger grain sizes.

The absolute values of the rotation and migration rates depend on time constants that are related to the atomistic events that occur during these two processes. It is interesting to note that the prefactor for rotation a_2 , determined by fitting the phase field model to the MD simulation results, is nearly an order of magnitude smaller than that for migration, a_1 . This suggests that the atomic processes associated with rotation involve greater transport distances or slower transport paths than those associated with migration. This is consistent with models for rotation that involve material transport over length scales comparable with defect spacings within the grain boundary and models for boundary migration that involve atomic hopping over length scales comparable with the boundary width.

Although the present simulation results demonstrate that grain rotation occurs simultaneously with grain boundary migration, the relative importance of these two effects for grain growth in polycrystalline structures of different grain size still requires further investigation. The MD results demonstrate that the grain rotation

occurs as a rigid body motion rather than by grain shearing by dislocation passage through the grain interior. The sharp interface limit of the phase field model is capable of capturing the general trends of boundary migration and grain rotation seen in the MD simulations, including the rotation rate dependence on grain size and the boundary migration rate dependence on misorientation.

Acknowledgements

M.U. and D.J.S. gratefully acknowledge the financial support of the Division of Materials Science of the Office of Basic Energy Sciences of the United States Department of Energy (Grant #FG02-88ER45367), under whose auspices this research was performed. This work was also supported by Department of Energy through the Computational Materials Science Network (CMSN) on *Fundamentals of Dirty Interfaces: From Atoms to Alloy Microstructures*. The authors acknowledge access to computing resources at the National Energy Research Scientific Computing Center (NERSC) via CMSN.

References

- [1] Smith CS. J Inst Metals 1948;74:747.
- [2] Weissmann S. In: Mueller WM, editor. Advances in X-ray analysis, vol. 2. New York (NY): University of Denver and Plenum Press; 1958. p. 47.
- [3] Fujita H. J Phys Soc Jpn 1961;16:397.
- [4] Hu H. Trans Am Inst Mining Eng 1962;224:75.
- [5] Li JCM. J Appl Phys 1962;33:2958.
- [6] Sandstrom R. Acta Metall 1977;25:897.
- [7] Doherty D, Szpunar JA. Acta Metall 1984;32:1789.
- [8] Gleiter H. Philos Mag 1969;20:821.
- [9] Shewmon PG. In: Margolin H, editor. Recrystallization, grain growth and textures. Metals Park (OH): American Society of Metals; 1966. p. 166.
- [10] Pond RC, Smith DA. Scripta Metall 1977;11:77.
- [11] Herrmann G, Gleiter H, Baro G. Acta Metall 1976;24:353.
- [12] Erb U, Gleiter H. Scripta Metall 1979;13:61.
- [13] Balluffi RW, Maurer R. Scripta Metall 1988;22:709.
- [14] Chan S-W, Balluffi RW. Acta Metall 1985;33:1113.
- [15] Chan S-W, Balluffi RW. Acta Metall 1986;34:2191.
- [16] King AH, Harris KE. In: Proceedings of the 2nd international conference on grain growth in polycrystalline materials, Kitakyushu, Japan; 1996.
- [17] Harris KE, Singh VV, King AH. Acta Mater 1998;46:2623.
- [18] Randle V, Brown A. Philos Mag A 1988;58:717.
- [19] Randle V, Brown A. Philos Mag A 1989;59:1075.
- [20] Randle V. Philoso Mag A 1993;67:1301.
- [21] Randle V. In: Proceedings of the 2nd international conference on grain growth in polycrystalline materials, Kitakyushu, Japan; 1996.
- [22] Randle V. Mater Sci Technol 1991;7:985.
- [23] Randle V, Ralph B. Proc R Soc Lond 1988;A415:239.
- [24] Read WT, Shockley W. Phys Rev 1950;78:275.
- [25] Martin G. Phys Stat Sol (b) 1992;172:121.
- [26] Cahn JW. In: Kaiser W, editor. Sintering of advanced ceramics, vol. 7. Westerville (OH): American Ceramic Society; 1990.
- [27] Chan S-W, Boyko VS. Phys Rev B 1996;53:16579.
- [28] Haslav AJ, Moldovan D, Phillipot SR, Wolf D, Gleiter H. Comput Mater Sci 2002;23.

- [29] Moldovan D, Wolf D, Phillpot SR. *Acta Mater* 2001;49:3521.
- [30] Raj R, Ashby MF. *Metall Trans* 1971;2:1113.
- [31] Moldovan D, Wolf D, Phillpot SR, Haslam AJ. *Acta Mater* 2002;50:3397.
- [32] Kobayashi R, Warren JA, Carter WC. *Physica D* 2000;140:141.
- [33] Upmanyu M, Smith RW, Srolovitz DJ. *Interf Sci* 1998;6:41.
- [34] Upmanyu M, Srolovitz DJ, Shvindlerman LS, Gottstein G. *Interf Sci* 1998;6:287.
- [35] Upmanyu M, Srolovitz DJ, Shvindlerman LS, Gottstein G. *Acta Mater* 1999;47:3901.
- [36] Srolovitz DJ, Upmanyu M. In: *International conference on recrystallization and grain growth*, Risoe, Denmark; 2000.
- [37] Kronberg ML, Wilson FH. *Trans Am Inst Mining Eng* 1949;185:501.
- [38] Lobkovsky AE, Warren JA. *Phys Rev E* 2001;63:051605.
- [39] Kobayashi R, Warren JA, Carter WC. *Physica D* 1998;119:415.
- [40] Warren JA, Carter WC, Kobayashi R. *Physica A* 1998;261: 159.